Acta Oncologica

ISSN: (Print) (Online) Journal homepage: www.tandfonline.com/journals/ionc20

Delineation atlas of the Circle of Willis and the large intracranial arteries for evaluation of doses to neurovascular structures in pediatric brain tumor patients treated with radiation therapy

L. Toussaint, S. Peters, R. Mikkelsen, S. Karabegovic, C. Bäumer, L. P. Muren, L. Tram-Henriksen, M. Høyer, Y. Lassen-Ramshad & B. Timmermann

To cite this article: L. Toussaint, S. Peters, R. Mikkelsen, S. Karabegovic, C. Bäumer, L. P. Muren, L. Tram-Henriksen, M. Høyer, Y. Lassen-Ramshad & B. Timmermann (2021) Delineation atlas of the Circle of Willis and the large intracranial arteries for evaluation of doses to neurovascular structures in pediatric brain tumor patients treated with radiation therapy, Acta Oncologica, 60:11, 1392-1398, DOI: 10.1080/0284186X.2021.1945679

To link to this article: https://doi.org/10.1080/0284186X.2021.1945679

ACTA ONCOLOGICA
2021, VOL. 60, NO. 11, 1392–1398
https://doi.org/10.1080/0284186X.2021.1945679

Taylor & Francis
Taylor & Francis Group

ORIGINAL ARTICLE

Delineation atlas of the Circle of Willis and the large intracranial arteries for evaluation of doses to neurovascular structures in pediatric brain tumor patients treated with radiation therapy

L. Toussaint[a,b], S. Peters[c], R. Mikkelsen[d], S. Karabegovic[d], C. Bäumer[e], L. P. Muren[a], L. Tram-Henriksen[f], M. Høyer[a], Y. Lassen-Ramshad[a]* and B. Timmermann[c,e]*

[a]Danish Centre for Particle Therapy, Aarhus University Hospital, Aarhus, Denmark; [b]Department of Clinical Medicine, Aarhus University, Aarhus, Denmark; [c]Department of Particle Therapy, University Hospital Essen, Germany; [d]Department of Neuroradiology, Aarhus University Hospital, Aarhus, Denmark; [e]West German Proton Therapy Centre Essen (WPE), West German Cancer Center (WTZ), Germany, German Cancer Consortium (DKTK); [f]Department of Pediatrics, Aarhus University Hospital, Aarhus, Denmark

ABSTRACT

Background: Survivors of pediatric brain tumors are susceptible to neurovascular disease after radiotherapy, with dose to the chiasm or Circle of Willis (CW) as risk factors. The aims of this study were to develop a delineation atlas of neurovascular structures, to investigate the doses to these structures in relation to tumor location and to investigate potential dose surrogates for the CW dose.

Material and methods: An atlas of the CW, the large intracranial arteries and the suprasellar cistern (SC) was developed and validated. Thirty proton plans from previously treated pediatric brain tumor patients were retrieved and grouped according to tumor site: 10 central, 10 lateralized, and 10 posterior fossa tumors. Based on the atlas, neurovascular structures were delineated and dose metrics (mean dose (D_{mean}) and maximal dose (D_{max})) to these structures and the already delineated chiasm were evaluated. The agreement between dose metrics to the CW vs. chiasm/SC was investigated. The minimal Hausdorff distance (HD_{min}) between the target and SC was correlated with the SC D_{mean}.

Results: The median D_{mean}/D_{max} to the CW were 53 Gy(RBE)/55 Gy(RBE) in the central tumors, 18 Gy(RBE)/25 Gy(RBE) in the lateralized tumors and 30 Gy(RBE)/49 Gy(RBE) in the posterior fossa tumors. There was a good agreement between the D_{max}/D_{mean} to the CW and the SC for all cases (R^2=0.99), while in the posterior fossa group, the CW D_{max} was underestimated when using the chiasm as surrogate (R^2=0.76). Across all patients, cases with $HD_{min} < 10$ mm between the target and the SC received the highest SC D_{mean}.

Conclusion: The pattern of dose to neurovascular structures varied with the tumor location. For all locations, SC doses could be used as a surrogate for CW doses. A minimal distance larger than 10 mm between the target and the SC indicated a potential for neurovascular dose sparing.

ARTICLE HISTORY
Received 16 May 2021
Accepted 16 June 2021

KEYWORDS
Neurovascular; pediatric brain tumors; proton therapy; Circle of Willis; suprasellar cistern; long-term effects

Background

Long-term survivors of pediatric brain tumors treated with radiation therapy are at an increased risk of developing cerebrovascular disease compared to the general population [1–4]. Damage to the major cerebral arteries of the brain, in part forming the Circle of Willis (CW), may lead to stenosis or occlusion of these large vessels. In the literature, stenosis and occlusive changes in patients treated with radiotherapy during childhood have been reported mostly in the proximal segment of the middle cerebral artery, the terminal part of the internal carotid artery as well as the anterior circulation of the CW [5–7]. Clinically, the patients may present with potentially life-threatening transient ischemic attacks, intracranial hemorrhages or ischemic strokes for which they remain at increased risk throughout their lifespan compared to their peers [1–4], affecting their quality of life.

Among other large collaborations such as the Pediatric Normal Tissue Effects in the Clinic (PENTEC) group [8], radiation-induced neurovascular late effects in pediatric brain tumor patients are currently being investigated in a prospective cohort study for the research EU-project 'HARMONIC' [9]. The latter study is investigating the extent and risk factors related to the development of neurovascular complications, quantifying radiation dose–volume relationships in neurovascular structures and exploring imaging changes as a precursor for neurovascular events.

Proton therapy is increasingly used for the treatment of pediatric brain tumors, as protons' physical properties allow for a reduction of the dose to normal tissues compared to conventional photon-based treatment, which could in turn reduce the risk of normal tissue complications [10]. However, neurovascular injury has been reported both after photon and proton irradiation [11].

CONTACT L. Toussaint lautou@rm.dk Danish Centre for Particle Therapy, Palle Juul-Jensens Boulevard 99, Aarhus N, 8200, Denmark
*The authors contributed equally to this work.

Supplemental data for this article can be accessed here.

Some proton-specific cohorts have been investigated [12–13], but as proton therapy is a relatively new modality, the follow-up period is not yet long enough to provide the full picture. Across both treatment modalities, radiation dose to certain brain structures (such as the CW or chiasm) was proposed as a risk factor for the development of neurovascular pathologies [7,13–16]. However, in clinical practice, neurovascular structures, such as the CW, are not systematically considered in radiotherapy planning (delineation and/or plan optimization). Although an atlas for the delineation of the CW based on T1 + contrast MRI-scan has been published [17], no guidelines independent of contrast media (i.e. using T2-weighted MRI) were proposed. In addition, no atlas was available for the exploration of the suprasellar cistern (SC) as a potential surrogate structure. Indeed, delineating brain arteries is a time-consuming task which makes it difficult to implement in a clinical workflow. Therefore, there is no consensus on which neurovascular structures to include for evaluation of the dose/volume relationship of radiation-induced neurovascular complications.

The aims of our study were therefore threefolded: to develop and validate a delineation atlas of neurovascular structures of interest (i.e. large intracranial vessels, the CW and the SC) for the HARMONIC project, to investigate the doses to these structures in relation to tumor location and to explore if doses to the chiasm or the SC, which might be easily contoured on a CT-scan, could be used as surrogate for the doses to the CW.

Material and methods

Delineation atlas

An atlas of the large intracranial arteries including all individual arteries of the CW, the first segment of the Middle Cerebral Artery (M1), the Internal Carotid Artery from the carotid canal level and the complete Basilar Artery was developed by neuroradiologists. Guidelines for the delineation of the SC, that is a suprasellar space containing among other structures the chiasm and the CW, were also established. The delineations of the cerebral arteries were based on T2 MRI-scans, while the SC was contoured both on CT- and T2 MRI-scans. Guidelines for the delineation process of the intracranial large vessels with illustrations of the relevant landmarks are proposed in Figure 1 and Supplementary Figure 1, while the SC delineations are shown in Supplementary Figure 2.

Validation of the delineation atlas

An intra-center validation of the atlas was performed in the Eclipse treatment planning system (version 13.7.16, Varian Medical System, Palo Alto, CA, USA). Three observers (neuroradiologist, radiation oncologist and medical physicist) were instructed to independently contour the 12 individual arteries and the CW from the standard clinical T2-weighted MRI, as well as the SC from a CT-scan for three example patients, based on the developed atlas. Of note, the chiasm was not included in the validation study as it is an established structure routinely delineated in clinical practice. The patients were chosen from the Danish Center for Particle Therapy database to represent the ideal scenario where the tumor is not located within the neurovascular structures of interest (i.e. two posterior fossa tumors, and a lateralized tumor), but no other selection criteria were applied. The similarity in the delineations of the three observers was assessed spatially as well as dose-wise (mean dose (D_{mean})/maximal dose (D_{max})). For the SC, the DICE similarity coefficients were calculated. For each patient, the symmetrical margin needed from the intersection volume of the three SC to encompass the three individual delineations was also investigated. This validation step was used for refining the contouring guidelines.

Exploration of doses to neurovascular structures depending on tumor location

After approval from the local ethical committee (19-9087-BO), the planning CT with the clinically approved structure set (including the chiasm delineation), rigidly registered planning MRI-scans (T2) as well as the delivered proton plan of 30 pediatric brain tumor patients previously treated with proton therapy at the West German Proton Therapy Center Essen (WPE, Essen, Germany) were retrieved. The patients were treated between February 2015 and June 2019, using scanning proton therapy. Two to four fields were used, to ensure that less than one-third of the fraction dose stopped in front of an organ at risk, and thereby reduce potential relative biological effectiveness (RBE) effects in normal tissues distal to the target volume. The treatment plans were grouped in three subcohorts, depending on tumor location: 10 central, 10 lateralized hemispheric, and 10 posterior fossa tumors. The characteristics of the patients are shown in Table 1.

For each patient, a single-observer applied the contouring atlas in treatment plans using the Raystation treatment planning system (version 9.2, RaySearch Laboratories AB, Stockholm, Sweden). The cerebral arteries and CW were contoured on T2-weighted MRI, while the SC was delineated both from the planning-CT and T2-weighted MRI independently (i.e. when delineating the CT-based SC, the observer did not look at the MRI-scan or SC).

For each structure of interest, the dose metrics (D_{mean}/D_{max}) were reported as a median value per group, for a constant RBE of 1.1. The agreement between dose metrics (D_{mean}/D_{max}) to the CW vs. the SC and to the CW vs. the chiasm was also evaluated by calculating their linear coefficient of determination R^2. When target volume and SC were not overlapping, the shortest distance between the structures was calculated as the minimal Hausdorff distance (HD_{min}) [18], and further related to the D_{mean} of the SC. For plans with whole-brain components, D_{mean} of the SC was calculated from the boost plan only.

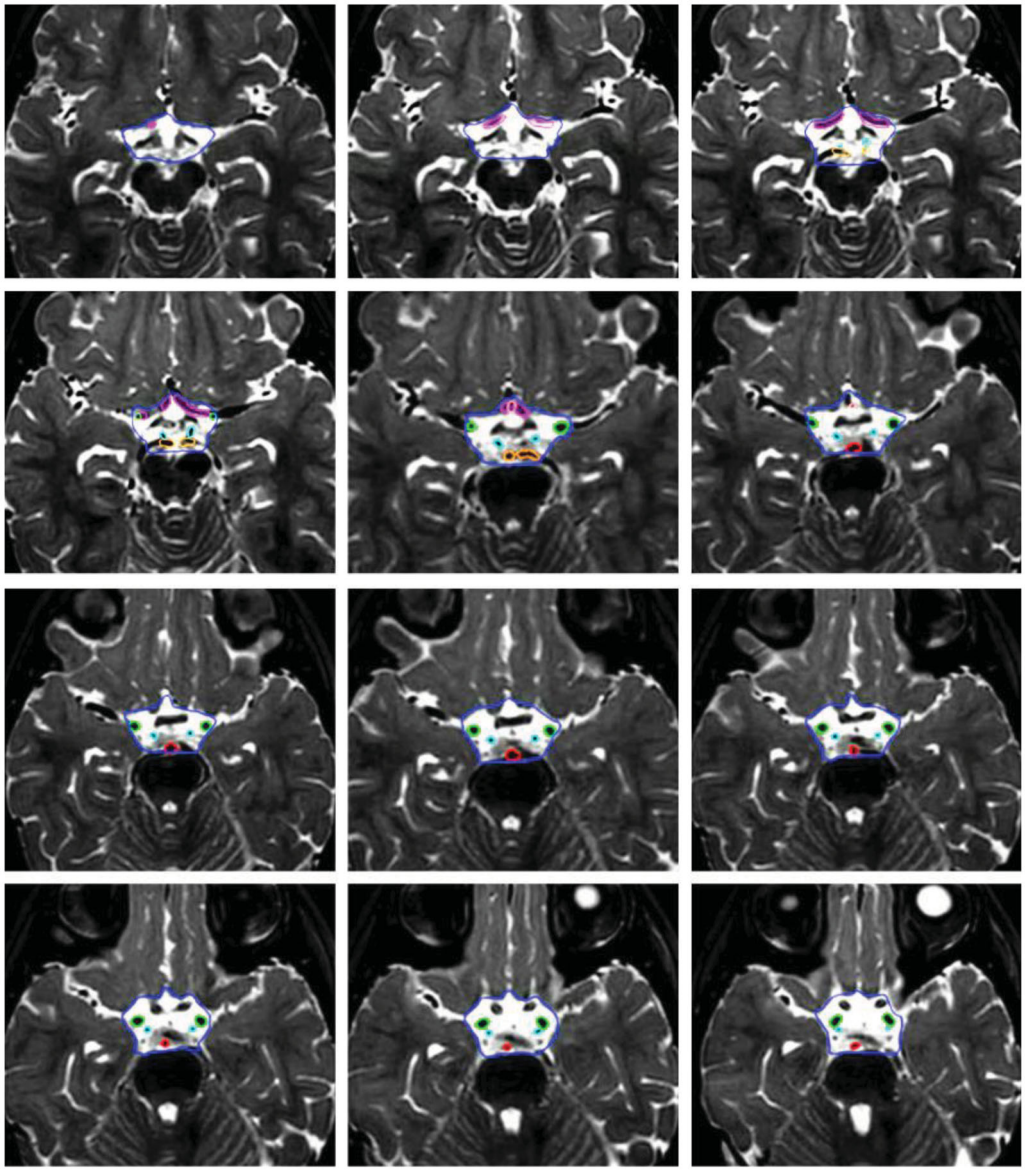

Figure 1. Slice-by-slice delineation of the SC as well as the individual arteries of the CW. The CW consists of the union of the first segment of the anterior cerebral arteries (ACA) via the anterior communicating artery (AComA), the terminal part of the internal carotid arteries (ICA), the posterior communicating arteries (PComA), the first segment of the posterior cerebral arteries (PCA) and the terminal part of the basilar artery (BA). The caudal extent of the CW is defined as the level at which PComA originates from ICA. The SC, filled with cerebrospinal fluid, extends cranially from the mammillary bodies and caudally to the bony limit of the sella turcica, and is anterior to the interpeduncular cistern and the brainstem. Its lateral limits follow the temporal lobes. The SC contains, among others, the arteries of the CW and the optic chiasm. Color code: AComA pink; ACA purple; ICA green; PComA cyan; PCA orange; BA red; SC dark blue.

Results

Validation of the delineation atlas

Examining inter-observer variation, visual assessment showed good spatial correlation between all individual arteries for all three patients, particularly in the cranio-caudal extent. This translated into comparable doses to the CW, both for D_{mean} and D_{max} (Table 2). At the individual arteries level, D_{mean} and D_{max} were also comparable across the three observers for the three cases, except for a few exceptions, for example, the right anterior cerebral artery and right posterior cerebral artery in Case 3 (Supplementary Tables 1 and 2). An illustration of the inter-observer differences in the contours of the SC and the CW is displayed in Supplementary Figure 3.

Larger variations were seen between the three observers in the delineation of the SC (with disagreement for the inferior border and lateral extent), leading to variations volume- and dose-wise (Table 2). In order to encompass all three delineations, the intersection volume of the three SC had to be symmetrically expanded by 0.7 cm (patients 1 and 3) and 1 cm (patient 2).

Exploration of doses to neurovascular structures depending on tumor location

Across all 30 patients, the median D_{mean}/D_{max} were 35 Gy(RBE)/52 Gy(RBE) to the CW. For the central tumors, the median D_{mean}/D_{max} were 53 Gy(RBE)/55 Gy(RBE) to the CW,

and all arteries received high doses mainly equal to the prescription dose due to the overlap with the target volume. In the lateralized tumors, the median D_{mean}/D_{max} were 18 Gy(RBE)/25 Gy(RBE) to the CW, and the contralateral arteries were in general spared from high doses. For the posterior fossa tumors, the median D_{mean}/D_{max} were 30 Gy(RBE)/49 Gy(RBE) to the CW, and the anterior arteries were spared from radiation dose, while the posterior arteries received higher doses due to the vicinity with the target volume. For example, the basilar artery, running along the

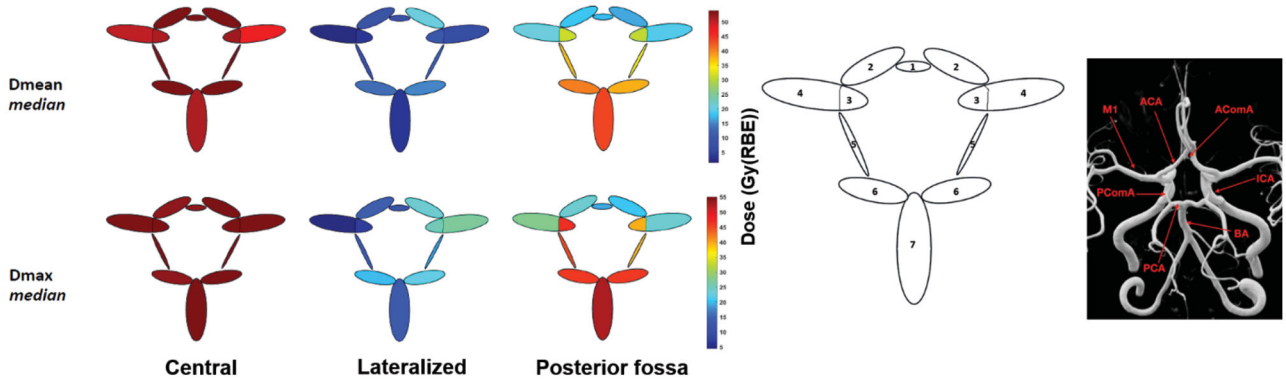

Figure 2. Median value of the D_{mean} (upper row) and D_{max} (lower row) to the CW cerebral arteries, grouped by tumor location (central, lateralized, posterior fossa). A schematic representation of the CW with its individual arteries labeled is shown in the middle. A 3D reconstruction of an MR-angiography of the CW with its individual arteries labeled is shown on the right, for reference. Nomenclature: 1 – ACA anterior communicating artery; 2 – AComA anterior cerebral artery L/R; 3 – ICA internal cerebral artery L/R; 4 – M1 first segment of the middle cerebral artery L/R; 5 – PComA posterior communicating artery L/R; 6 – PCA posterior cerebral artery L/R; 7 – BA basilar artery.

Table 1. Summary of the characteristics of the entire patient cohort, as well as in the three specific groups.

Patient group	Gender	Median age at PT start [range] (years)	Diagnosis N	Residual disease at PT start	Median prescription dose [range] (Gy(RBE))	Number of CSI patients; boost dose (Gy(RBE))
All patients (*N* = 30)	13F/17M	7.1 [1.2–16.6]		Yes 18/30	54 [40–59.4]	8
Central (*N* = 10)	5F/5M	11.3 [5.4–16.4]	Craniopharyngioma 4 Low-grade glioma 2 High-grade glioma 1 Germ-cell tumors 3	Yes 9/10	54 [40–59.4]	2[a]; boost dose 16 Gy(RBE)
Lateralized (*N* = 10)	4F/6M	4.6 [2.4–14.6]	Ependymoma 4 Low-grade glioma 2 High-grade glioma 1 Other embryonal tumors 1 ATRT 2	Yes 5/10	55.6 [54–59.4]	2; boost dose 30.6 Gy(RBE) and 19.8 Gy(RBE)
Posterior fossa (*N* = 10)	4F/6M	3.8 [1.2–16.6]	Ependymoma 4 Low-grade glioma 1 Medulloblastoma 4 ATRT 1	Yes 4/10	54 [50.4–59.4]	4; boost doses 30.6 Gy(RBE))

Abbreviations: N: number of patients; F: female; M: male; PT proton therapy; ATRT Atypical Teratoid Rhabdoid Tumor; CSI: craniospinal irradiation.
[a]One patient received whole-ventricular irradiation instead of CSI.

Table 2. Dose and volume metrics for the validation of the delineation atlas, for the CW (left) and the SC (right).

	CW		SC			
Observer	D_{mean} (%prescription dose)	D_{max} (%prescription dose)	D_{mean} (%prescription dose)	D_{max} (%prescription dose)	Volume (cm^3)	DICE
Case 1						
1	69.4	92.1	71.5	96.1	5.6	0.76*
2	68.1	92.2	70	94.7	4.6	0.81**
3	68.3	91.2	66.4	95.5	6.3	0.76***
Case 2						
1	19.8	72.6	15.7	88.2	6.8	0.83*
2	18.9	72.7	14	73.3	8.9	0.86**
3	17.8	72.8	17.1	81.5	8.7	0.84***
Case 3						
1	4.7	47.3	1.3	29	3.4	0.75*
2	5	47	3.1	52.5	4.3	0.67**
3	3.7	42.7	2	36.1	5.8	0.70***

The dose metrics are expressed in percentage of the prescription dose.
DICE coefficients are calculated for * observer 1 vs. 2 ** observer 2 vs. 3 *** observer 1 vs. 3.

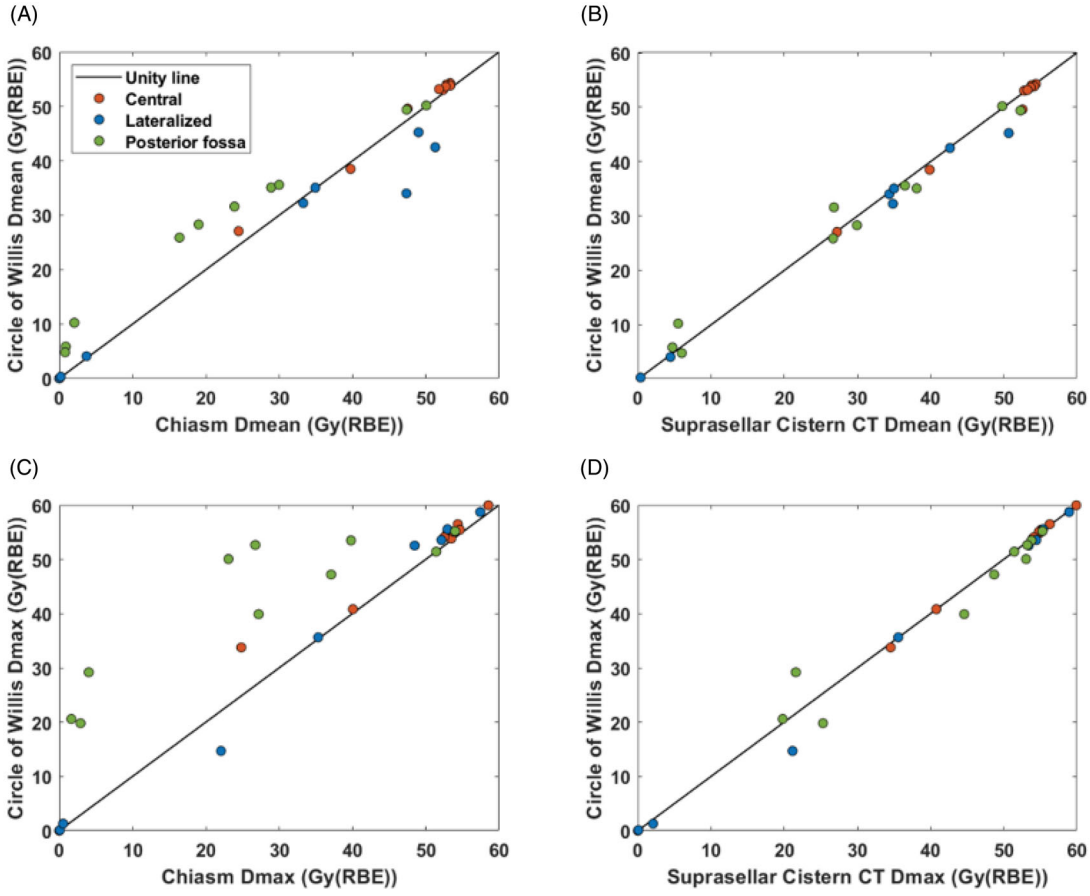

Figure 3. Agreement between D_{mean} (upper row) and D_{max} (lower row) to the CW and its potential surrogates (chiasm left, SC (CT-scan delineations) right). A good agreement exists when the individual data points fall on the unity line. Each group is represented by a specific color.

brainstem, received the highest doses in these tumors with a median D_{mean}/D_{max} of 44 Gy(RBE)/53 Gy(RBE) (Figure 2).

The SC volumes from the delineations based on MRI were in general slightly larger than the volumes from the CT delineations (R^2=0.92) (Supplementary Figure 4). Dose-wise, D_{mean}/D_{max} were in agreement between the CT and MRI delineations, with the individual data points falling on the unity line for all three groups and a linear coefficient of determination R^2 of 0.99 for both metrics (Supplementary Figure 4).

Looking at potential surrogates for estimating the dose to the CW, for the three locations, there was a good agreement between the D_{max}/D_{mean} to the CW and the SC (delineated on CT) (R^2=0.99 for both metrics, for the whole cohort) (Figure 3(B, D)). For the D_{max}, a few deviations were seen for three patients at relatively low D_{max} values. The agreement between D_{max} to the CW and the chiasm was good for the central (R^2=0.97) and lateral (R^2=0.99) groups, while in the posterior group, the CW D_{max} was consistently underestimated when using the chiasm as surrogate (R^2=0.78) (Figure 3(C)). In the whole cohort, this translated in a R^2 of 0.95 for D_{mean}, and 0.83 for D_{max} when comparing the chiasm doses to the CW doses (Figure 3).

Across all 30 patients, cases with HD_{min} lower than 10 mm between the target and the SC (delineated on CT) received the highest D_{mean} to the SC. For all central tumors, the SC and target were overlapping and for all but two cases, SC D_{mean} was equal to the prescription dose. In the lateralized tumors, cases with a HD_{min} larger than 20 mm between the target and SC had a SC D_{mean} of 0 Gy(RBE). In the posterior fossa tumors, all cases had a HD_{min} lower than 14 mm, and half of these cases had a SC D_{mean} of at least half the prescription dose (for $HD_{min} < 1$ mm) (Supplementary Figure 5).

Discussion

Neurovascular complications after radiotherapy treatment of pediatric brain tumors are an important issue, potentially affecting patients' quality of life. In this study, we developed and validated a detailed atlas for the delineation of neurovascular structures of interest. The guidelines allowed for reproducible delineation of the larger intracranial arteries and the CW. Overall we found that the doses delivered to neurovascular structures varied with the tumor location, and we were able to describe group-specific patterns and dose ranges. Our data indicated that the doses to the SC could be used as a surrogate for the dose to the CW for all tumor locations and that a minimal distance of more than 10 mm between the target and the SC could indicate a potential for dose sparing. When performing the intra-institutional atlas validation, we did not compare volumes or DICE coefficients for the delineated individual arteries as usually recommended [19], as their volumes were very small (<0.1 cm^3). We therefore included a comparison of doses to assess the

delineations of the three observers, as it would also be the relevant metric for further development of dose/volume relationships of radiation-induced neurovascular pathologies: good agreement between dose metrics would illustrate consistent inter-observer delineations.

A visual assessment of the inter-observer delineations was performed slice-by-slice for all the delineated structures (individual arteries, CW and SC). Lateral differences were seen in the extent of the individual arteries, while the cranio-caudal limits were consistent across all three observers. The lateral differences were due to different technique in the delineation process: two of the observers were delineating on the transversal view only, while the third one was combining the transversal and coronal plane, sometimes resulting in non-continuous structures in some cases expanding more laterally. This translated into slight dose differences between observers for those arteries, as seen for, for example, the right anterior cerebral artery and right posterior cerebral artery in Case 3 (Supplementary Tables 1 and 2), despite the uncertainties inherent to dose assessment in very small structures. However, the differences were overall small and did not result in substantial dose differences, as seen with the similar values of D_{mean}/D_{max} for the whole CW across the three observers.

The largest variations in delineations were seen for the SC, with differences in the lateral extent but also in the limit along the brainstem, due to the inclusion of the interpeduncular cistern in some cases. This observation was used to refine the delineation guidelines, and to provide more precise landmarks for the contouring of the SC (e.g. exclusion of the interpeduncular cistern). Despite the observed variations this had in terms of dose, this should not have an impact on the use of the SC dose as surrogate for the CW dose. Indeed, the exploration of surrogate dose was performed on the 30 independent patients where the delineation of the SC followed the current definition of the atlas.

Overall, we demonstrated the generalized applicability of the atlas. The three observers achieved good agreement (after visual inspection, and dose-wise) in the contouring of individual arteries when following the proposed guidelines, despite very different backgrounds. The degree of experience of the three observers varied in terms of use of the delineation software, but also in their neuroanatomy training.

For the exploration of doses, the delineations of the 30 patients were done by a single observer, thereby removing inter-observer variability in the dose metrics assessment. As the intra-center validation revealed good agreement between the three observers in the delineation of all individual arteries, we would not expect the dose analysis results to be different if different observers were delineating the neurovascular structures of interest. However, it could be of interest to perform a larger validation across a number of pediatric radiotherapy centers in order to confirm this hypothesis.

Despite the good reproducibility in the delineation of the CW, this task is tedious and might therefore not be realistically implementable in a clinical workflow. Therefore, the definition of a dose surrogate might help with locating the area of interest for neurovascular structures and guide future treatment planning. We studied both the dose to the chiasm [13] (structure routinely delineated in all brain tumor patients) and to the SC (that includes all individual arteries of the CW) as a surrogate for the CW dose. The SC location as a function of target could also be studied, because location metrics are more easily calculable between two continuous surfaces (i.e. target and SC), while the CW was non-continuous per definition. In addition, contrary to the arteries, the SC is visible both on CT and MRI and we could confirm similarity between CT and MRI contours dose- and volume-wise. The SC contoured from CT-scans could therefore easily be used for further assessments.

In the literature, dose to the optic chiasm ($D_{max} \geq 54$ Gy(RBE)) has been shown to be a predictor of the development of vasculopathy in a cohort of pediatric brain tumor patients treated with proton therapy [13]. We found a potential underestimation of the dose to the CW when the chiasm dose was used as a surrogate, especially for posterior fossa cases. This observation is confirmed anatomically as the SC has a larger volume than the chiasm and encompasses the whole CW, whereas the chiasm is located more toward the anterior part of CW. The largest dose differences between the CW and the chiasm were seen for the posterior fossa cases, where most of the dose is delivered to the posterior part of the CW (namely to the basilar artery, posterior cerebral arteries and posterior communicating arteries - Figure 2). However, while we demonstrated that the SC could be a better dose surrogate for the dose to the CW, the clinical applicability remains to be prospectively investigated. In the HARMONIC study, the association between the incidence of neurovascular impairment and radiation dose to the SC, the CW and the large arteries will be further explored.

El Fayech et al. showed that D_{mean} to the CW was a predictor of stroke, for D_{mean} as low as 10 Gy [14]. In our 30 patients, only eight were below this threshold. Haddy et al. suggested a linear increase in the risk of death from cerebrovascular disease with the dose delivered to the prepontine cistern [16]. This cistern contains the basilar artery, and in our 30 patients, the dose to the basilar artery was particularly high, especially in the central and posterior fossa groups. Both of these observations could indicate that particular attention should be given in patients' follow-up regarding neurovascular complications.

In terms of doses delivered to the neurovascular structures, group-specific patterns could be described. For the central tumors, the SC and target volume were fully overlapping, resulting in all arteries receiving the prescription dose. The lateralized was the group with the lowest doses to the CW, as the distance between the SC and target volume was the largest ($HD_{min} > 20$ mm for half cases). The anterior arteries of the posterior fossa cases were exposed to high doses, because of small distances between the SC and target volume ($HD_{min} < 14$ mm, and as small as 1 mm). When looking at the potential for neurovascular structures sparing, the doses in the posterior fossa and central tumors appeared difficult to optimize further due to the very close vicinity between the SC and the target. Overall, a HD_{min} larger than

10 mm between the target and the SC could be a threshold for potential neurovascular structures sparing.

It should be noted that a fixed RBE of 1.1 was used in this study (as is the case clinically), and therefore the potential variations in the RBE along the beam axis were not taken into account [20]. However, when using the SC dose as a surrogate for the CW dose, we would not expect RBE dose differences to modify our conclusions as the location of both structures is almost similar (however, the volume differs). Therefore, a potential increase in dose in one structure would probably translate in an increase of the same magnitude in the other structure. In addition, the use of multiple fields in treatment planning reduces the potential distal-edge effect in sensitive normal tissues.

Finally, our study is based exclusively on proton therapy dose distributions. A comparison between photon- and proton-specific dose patterns could prove informative regarding the expected differences in the incidence of neurovascular impairment depending on treatment modality.

In summary, we developed and internally validated an atlas for delineation of neurovascular structures of interest, allowing us to further study their group-specific dose patterns. Our data indicate that the doses to the SC can be used for all tumor locations as a surrogate for the dose to the CW. As this structure is easily identifiable on CT-scans, it could facilitate the inclusion of neurovascular considerations in the radiotherapy process. Overall, this knowledge might further guide the treatment planning process in an effort to spare neurovascular structures.

Disclosure statement

No potential conflict of interest was reported by the author(s).

Funding

The HARMONIC project (Health effects of cArdiac fluoRoscopy and MOderN radIotherapy in paediatriCs) has received funding from the Euratom Research and Training Programme 2014-2018 under grant agreement No 847707. This publication reflects only the authors' view and the European Commission is not responsible for any use that may be made of the information it contains.

References

[1] Mueller S, Sear K, Hills NK, et al. Risk of first and recurrent stroke in childhood cancer survivors treated with cranial and cervical radiation therapy. Int J Radiat Oncol Biol Phys. 2013;86(4):643–648.

[2] Bowers DC, Liu Y, Leisenring W, et al. Late-occurring stroke among long-term survivors of childhood leukemia and brain tumors: a report from the Childhood Cancer Survivor Study. J Clin Oncol. 2006;24(33):5277–5282.

[3] Nordstrom M, Felton E, Sear K, et al. Large vessel arteriopathy after cranial radiation therapy in pediatric brain tumor survivors. J Child Neurol. 2018;33(5):359–366.

[4] Van Dijk IWEM, Van der Pal HJH, Van Os RM, et al. Risk of symptomatic stroke after radiation therapy for childhood cancer: a long-term follow-up cohort analysis. Int J Radiat Oncol Biol Phys. 2016;96(3):597–605.

[5] Brant-Zawadzki M, Anderson M, DeArmond SJ, et al. Radiation-induced large intracranial vessel occlusive vasculopathy. Am J Roentgenol. 1980;134(1):51–55.

[6] Scala M, Fiaschi P, Cama A, et al. Radiation-induced moyamoya syndrome in children with brain tumors: case series and literature review. World Neurosurg. 2020; 135:118–129.

[7] Omura M, Aida N, Sekido K, et al. Large intracranial vessel occlusive vasculopathy after radiation therapy in children: clinical features and usefulness of magnetic resonance imaging. Int J Radiat Oncol Biol Phys. 1997;38(2):241–249.

[8] Constine LS, Olch AJ, Jackson A, et al. Pediatric Normal Tissue Effects in the Clinic (PENTEC): an international collaboration to assess normal tissue radiation dose-volume-response relationships for children with cancer. Int J Radiat Oncol Biol Phys. 2021.

[9] Harmonic: Health effects of cardiac fluoroscopy and modern radiotherapy in paediatrics [Internet]. Barcelona: ISGlobal; [cited 2021, June 15]. Available from: https://harmonicproject.eu/

[10] Journy N, Indelicato DJ, Withrow DR, et al. Patterns of proton therapy use in pediatric cancer management in 2016: an international survey. Radiat Oncol. 2019; 132:155–161.

[11] Bavle A, Srinivasan A, Choudhry F, et al. Systematic review of the incidence and risk factors for cerebral vasculopathy and stroke after cranial proton and photon radiation for childhood brain tumors. Neurooncol Pract. 2021;8(1):31–39.

[12] Kralik SF, Watson GA, Shih CS, et al. Radiation-induced large vessel cerebral vasculopathy in pediatric patients with brain tumors treated with proton radiation therapy. Int J Radiat Oncol Biol Phys. 2017;99(4):817–824.

[13] Hall MD, Bradley JA, Rotondo RL, et al. Risk of radiation vasculopathy and stroke in pediatric patients treated with proton therapy for brain and skull base tumors. Int J Radiat Oncol Biol Phys. 2018;101(4):854–859.

[14] El-Fayech C, Haddy N, Allodji RS, et al. Cerebrovascular diseases in childhood cancer survivors: role of the radiation dose to Willis Circle arteries. Int J Radiat Oncol Biol Phys. 2017;97(2):278–286.

[15] Mueller S, Fullerton HJ, Stratton K, et al. Radiation, atherosclerotic risk factors, and stroke risk in survivors of pediatric cancer: a report from the Childhood Cancer Survivor Study. Int J Radiat Oncol Biol Phys. 2013;86(4):649–655.

[16] Haddy N, Mousannif A, Tukenova M, et al. Relationship between the brain radiation dose for the treatment of childhood cancer and the risk of long-term cerebrovascular mortality. Brain. 2011;134(5):1362–1372.

[17] Scoccianti S, Detti B, Gadda D, et al. Organs at risk in the brain and their dose-constraints in adults and in children: a radiation oncologist's guide for delineation in everyday practice. Radiother Oncol. 2015;114(2):230–238.

[18] Taha AA, Hanbury A. Metrics for evaluating 3D medical image segmentation: analysis, selection, and tool. BMC Med Imaging. 2015; 15:29.

[19] Vinod SK, Jameson MG, Min M, et al. Uncertainties in volume delineation in radiation oncology: A systematic review and recommendations for future studies. Radiother Oncol. 2016;121(2):169–179.

[20] Paganetti H. Relative biological effectiveness (RBE) values for proton beam therapy. Variations as a function of biological endpoint, dose, and linear energy transfer. Phys Med Biol. 2014;59(22):R419–R472.